Recommended Paper

BAAS: Backscatter as a Sensor for Ultra-Low-Power Context Recognition

Yoshihiro Nakagawa[1,a)] Toru Maeda[1] Akira Uchiyama[1,b)] Teruo Higashino[1,c)]

Received: May 10, 2021, Accepted: November 2, 2021

Abstract: Context recognition has attracted attention for various daily life applications. Many existing approaches use micro-electromechanical systems (MEMS) sensors which require additional silicon chips to process and transmit the sensor data. The energy consumption of such components is relatively large, requiring maintenance for charging or replacing batteries. In this paper, we propose *BAAS*: a novel concept using Backscatter As A Sensor. BAAS recognizes contexts using a frequency shift backscatter tag with ultra-low power consumption. The key components of the backscatter tag are an oscillator and a motion switch. The state of the motion switch changes according to the movement of humans or the change of the situation of things. While the motion switch is on, the energy is supplied to the oscillator, and the frequency of the backscattered signal shifts according to the oscillation frequency of the oscillator. Context recognition is achieved by observing the existence and absence of the frequency shift. To demonstrate the feasibility of context recognition using the backscatter tag, we have implemented a prototype and evaluated its performance. Our results show that we can detect the frequency shift by BAAS within 3 m, backscattering BLE signal from an exciter implemented by a commodity device.

Keywords: wireless sensing, context recognition, backscatter, frequency modulation

1. Introduction

Context recognition has attracted many researchers for various daily life applications. For example, in elderly care, the detection of leaving bed reduces the burden on caregivers [1]. The detection of opening and closing doors and windows is useful for adaptive control of air conditioning and intrusion detection [2]. Also, some monitoring services are available by monitoring the use of things such as electric pots and remote controllers [3].

Many existing approaches for context recognition use MEMS sensors such as accelerometers and gyroscopes [4], [5]. However, they require further processes like analog-to-digital conversion, modulation, and wireless data transmission, which consume relatively large amounts of energy [6]. Therefore, batteries are usually used to meet the energy requirement. To avoid the maintenance cost of the batteries, energy harvesting is widely used combined with power saving. Such products are available on the market [*1]. However, since the amount of harvested energy is small, most approaches limit device capability such as operation frequency by duty cycling. This means devices with energy harvesting are essentially not suitable for applications involving high-frequency operations (e.g., activity recognition).

Another approach is to make wireless data transmission ultra-low-power since it is the most energy-consuming process. Recently, researchers have revealed the capability of backscatter communication using existing RF signals such as Wi-Fi, Bluetooth, LoRa, and TV [6], [7], [8] for IoT (Internet-of-Things) devices. Backscatter is a communication technology consisting in switching the reflection/absorption state of surrounding RF signals. As backscatter does not need to generate a carrier signal on the tag, it can transmit data for context recognition with ultra-low power (e.g., on the order of micro-watts [8]). Nevertheless, it still requires the processing of sensor data, i.e., analog-to-digital conversion and modulation by an A/D converter and a microcontroller. Implementing such digital components requires careful hardware and software designs considering the energy consumption of the whole system, which is complicated for many developers and researchers without deep knowledge of them. Moreover, additional components increase implementation cost, which is not desirable to deploy sensors everywhere.

To address these challenges, we propose a context recognition platform named *BAAS* – Backscatter As A Sensor. BAAS does not use backscatter to transmit sensor data but as a sensor. The key component of BAAS is a frequency shift backscatter tag which consists of an antenna, an RF switch, an oscillator, and a motion switch. We note that it does not require a microcontroller. In contrast to existing backscatter communication, the tag embeds the state of the motion switch into the frequency domain. While the motion switch is on, the energy is supplied to the oscillator to make a frequency shift in the backscattered signal. The

[1] Graduate School of Information Science and Technology, Osaka University, Suita, Osaka 565–0871, Japan
[a)] y-nakagawa@ist.osaka-u.ac.jp
[b)] uchiyama@ist.osaka-u.ac.jp
[c)] higashino@ist.osaka-u.ac.jp

The preliminary version of this paper was published at Multimedia Communication and Distributed Processing System Workshop (DPSWS 2020), November 2020. The paper was recommended to be submitted to Journal of Information Processing (JIP) by the chief examiner of SIGDPS.

[*1] https://www.enocean.com/en/technology/energy-harvesting/

shifting frequency depends on the oscillation frequency. Therefore, we leverage the oscillation frequency as the identification of the tags as well as the frequency modulation. The state of the motion switch changes according to the movement of humans or the change of the situation of things. Context recognition is achieved by observing the existence of this frequency shift and its change over time. Contrary to many existing approaches for context recognition, machine learning is not necessary because the existence of the frequency shift directly corresponds to ON/OFF of the motion switch which is related to the context. Furthermore, if a pair of an oscillation frequency and its corresponding context with the target person/object is known in advance, the target is identified according to the shift frequency.

The oscillator used in our tag operates with μW level power consumption [*2]. Therefore, a coin cell is enough for a lifetime of several years as wristwatches. A permanent lifetime is further expected by energy harvesting. However, to reduce the power consumption of the oscillator, it is necessary to suppress the oscillation frequency to several hundred kHz. This means since the channel bandwidth of Wi-Fi and Bluetooth is on the order of MHz, the frequency shift of several kHz is not enough to avoid the effect of the noise. To overcome the problem, BAAS employs Interscatter [7] to emit a narrow-band carrier signal by Bluetooth Low Energy (BLE). In this paper, we design the backscatter tag with an evaluation of its fundamental performance.

Our contributions are summarized below.

- We designed a backscatter tag without a microcontroller and proposed BAAS, a novel platform using backscatter as a sensor for context recognition.
- The backscatter tag is ultra-low-power, which does not need to limit the frequency of operation and communication for power saving contrary to the existing methods. Therefore, BAAS is also useful for applications involving high-frequency operations (e.g., activity recognition).
- Context recognition using the backscatter tag does not require learning data collection since it does not rely on machine learning. Instead, we recognize pre-defined contexts by observing the existence of the corresponding frequency shifts. Since we do not rely on machine learning, BAAS is robust to the environment change.
- We have implemented a prototype of the backscatter tag and confirmed its feasibility for context recognition through performance evaluation in a real environment with the demonstration of concept applications.

2. Related Work

2.1 Context Recognition by MEMS Sensors

The research community has explored a number of ways to recognize context from wearable sensor data. The mainstream of the context recognition is to use MEMS sensors such as an accelerometer and a gyroscope with high accuracy and resolution [9]. However, they depend on devices such as smartwatches which require frequent battery charge or replacement.

To solve the problem, there are many methods for low-power context recognition using a barometric pressure sensor [10], low-sampling rate acceleration [11], the amount of power generated from human motions [12], and so on. They focus on the sensing part without sending the sensed data while wireless data transmission is the most energy-consuming process. Therefore, we need an integrated design from sensing to transmission.

2.2 Wi-Fi CSI

Recently, context recognition using Wi-Fi CSI (Channel State Information) has been actively studied [13], [14], [15], [16] because it works by using commodity Wi-Fi devices. In Ref. [16], the authors proposed two models for quantitatively correlating CSI dynamics and human activities: a CSI-speed model that correlates CSI dynamics with the movement speed and a CSI-activity model that correlates the movement speed of different body parts with a specific activity. FallDeFi [17] extracts the spectrogram of CSI by Short Time Fourier Transform (STFT) combined with noise filtering by PCA and DWT (Discrete Wavelet Transform) for accurate fall detection. MultiSense [18] achieves the respiration monitoring of multiple persons by Independent Component Analysis (ICA) to separate the mixed signals. Widar3.0 [19] recognizes gestures by extracting body-coordinate velocity profiles based on estimated body orientation to achieve cross-domain recognition. Guo et al. [20] achieved individual identification and workout assessment by using CSI autocorrelation and DNN. Wi-Fi CSI is also capable of soil moisture sensing as presented in Strobe [21] which exploits the relative Time of Flight (ToF) by using multiple antennas.

However, most of the approaches require model training for each target environment. Also, the separation of multiple targets is essentially difficult, especially for multiple moving targets. On the other hand, BAAS enhances Wi-Fi CSI sensing capability by attaching a simple backscatter tag to the targets, which enables target identification and the sensing of the target state coupled with the motion switch. Specifically, BAAS can directly recognize the target states without any learning process.

2.3 RFID

Another approach for maintenance-free context recognition is passive RFID. Since RFID phase information is more reliable than the Wi-Fi CSI, many approaches are based on fundamental physics related to the wavelength, the distance, and the phase. In this sense, context recognition by RFID is more accurate and precise than Wi-Fi CSI. Another advantage of RFID tags is their inherent ability to identify targets (i.e., attached parts, subjects, or objects) by responding with its identification.

Super low-resolution accelerometers are proposed in Ref. [1], which converts acceleration into the change of IDs reported from a single RFID tag. To achieve real-time gesture recognition, EU-IGR [22] proposed an LSTM-based sequence labeling classifier that predicts gestures before its completion by using two tags attached on each arm. RF-Kinect [23] recognizes 3D body movement by attaching multiple tags on the subject's body. It employs phase difference between tags (PDT) to track the body movement, which is robust to antenna orientation change. RF-Wear [24] recognizes body pose with tag arrays on each joint by observing the

[*2] The oscillator of SiTime SiT1569 generates frequencies up to 462.5 kHz with μW level power consumption.

phase difference between the signals from the tags. RF-ECG [25] estimates heart rate variability with a tag array attached on the chest by separating chest movement due to respiration and heartbeat. Interestingly, Tagtag [26] is a method for material sensing using two tags on a container, leveraging material-dependent phase change (i.e., antenna impedance changes). Also, soil moisture sensing is possible by attaching two tags on each pot based on signal change due to soil moisture [27].

Most of the above methods require the collection of training data, which is dependent on the target environment. Compared with RFID-based methods, BAAS can directly recognize predefined contexts without any data collection for training. Also, if future smart wireless devices have a capability of Software Defined Radio (SDR), we can directly use them with the addition of the backscatter tags that can be easily developed by users.

2.4 Backscatter Communication

Various backscatter communication techniques have been proposed following the pioneering concept of the ambient backscatter [6]. Ambient backscatter achieves wireless communication with ultra-low power by switching the antenna state between reflecting and absorbing RF signals existing in the environment such as TV. However, the communication distance is still limited. On the other hand, Ref. [28] eliminates the self-interference to extend the communication range. Reference [29] proposed a method to increase the backscatter communication range and speed by using multiple antennas. Also, Wi-Fi backscatter [8] achieves a maximum communication speed of 1 kbps and a maximum communication range of 2.1 m. Passive Wi-Fi [30] achieves a communication distance of 100 feet at a rate up to 11 Mbps by controlling RF transmitted by the base station.

Such backscatter communication techniques are key enablers for the spread of IoT devices combined with energy harvesting. Nevertheless, it still requires sensor data processing by an A/D converter and a microcontroller. Implementing such digital components requires careful hardware and software designs, considering the whole system's energy consumption, which is complicated for many developers and researchers without in-depth knowledge. Moreover, additional components increase implementation cost, which is not desirable for pervasive IoT devices.

2.5 Context Recognition Using Backscatter Sensors

The concept of leveraging backscatter as a sensor has recently attracted researchers due to its low implementation cost and battery-free or ultra-low-power operation.

In Printed Wi-Fi [31], a 3D printer is used to create an antenna using a conductive material. Printed Wi-Fi generates the change of the antenna impedance by turning a physical switch ON/OFF according to various physical movements such as wind and water flow. Hence, it switches between the two states of reflection and absorption of the Wi-Fi signal, converting physical movements into the RF signal change. Printed Wi-Fi is advantageous in terms of energy since it does not require any power, generating backscatter signals by rotating gears using forces such as wind and water flow. However, it does not focus on context recognition, especially on human activities. This is challenging because the frequency of the backscatter signals generated by human motions is similar to the RF signal change due to the human motions themselves. Therefore, the backscatter signals are indistinguishable from the signal changes due to the human motions. LiveTag [32] is a chip-less touch interface that leverages printed resonators and antennas to make the signatures of touch events in the Wi-Fi spectrum. The above approaches are completely battery-free. However, the communication range is very limited, like up to 1 m, and capturing the human motions is essentially difficult.

Some others add a small amount of energy (μW level) to enhance backscatter sensors' capability, assuming energy harvesting. Specifically, a small amount of energy enables frequency shift, which can avoid interference with the carrier wave frequency, extending the backscatter communication distance. UbiquiTouch [33] is an ultra-low-power wireless touch interface that embeds the information on a touch point in a frequency-modulated bit sequence. Daskalakis et al. [34] presented soil moisture sensing by generating a frequency shift in the backscattered signal using a CSS555 timer. RF Bandaid [35] proposed an RF sensing platform (RFSP) which consists of an energy harvester, an antenna, an oscillator, an RF switch, and a resistive or capacitive sensor. The resistive or capacitive sensor changes its resistance or capacitance according to its sensing target. For example, the capabilities of temperature, force, and stress measurements have been demonstrated in Ref. [35]. RF Bandaid employs a micropower precision programmable oscillator (MPPO) from Linear Technology LTC6906. This oscillator converts the resistance or capacitance of the sensor to a specific frequency. The RF switch changes its state according to the oscillator frequency, resulting in the frequency shift in the backscattered signal.

BAAS also leverages a small amount of energy for the frequency shift to extend the communication range. Moreover, the frequency shift helps separate the backscattered signal from the RF signal changes due to human motions. BAAS is also unique in its analog design based on the motion switch, which is directly coupled with the target context's state.

3. System Overview

Figure 1 illustrates the system overview. An exciter emits RF signal for backscatter tags attached to people and objects such as shoes, doors, and chairs. A receiver then observes a frequency spectrum to detect the existence of the tags and the state of the motion switches which are coupled with corresponding contexts. We assume devices with power supply or large batteries such as smartphones, laptops, and Wi-Fi base stations as exciters and receivers. To use off-the-shelf devices as receivers, we need an

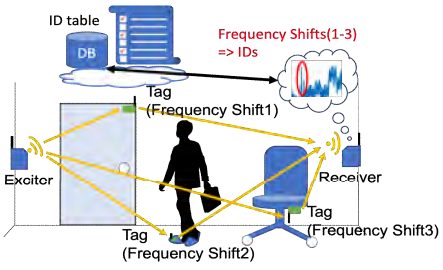

Fig. 1 System overview.

additional device such as SDR and a spectrum analyzer. Some products are available on the market such as Analog Devices ADALM-PLUTO which costs 200 USD.

If the backscatter tag exists in the target environment with its motion switch turned on, the frequency shift corresponding to the frequency of the carrier signal f_c appears in the backscattered signal. We assume a pair of the oscillation frequency f_i of tag_i and the corresponding context c_i of the tag is registered in a database. The receiver detects peaks in the frequency spectrum and determines whether there is a frequency shift f_i or not. If the peak at f_i is detected, we recognize the occurrence of c_i.

4. System Design and Implementation

4.1 Design of Frequency Shift Backscatter Tag

Figure 2 shows a block diagram of the frequency shift backscatter tag composed of an oscillator, an RF switch, an antenna, a motion switch, and a battery (or an energy harvester). The human movement or the state change of an object turns the motion switch on and off. When the motion switch is on, current flows in the circuit. Then, the RF switch connected to the antenna turns on and off at the oscillator frequency of f_i mounted on the backscatter tag i. The impedance of the antenna is switched according to the state of the RF switch, generating a frequency shift of f_i Hz in the backscattered signal. This is explained by basic trigonometry:

$$2 \sin f_c t \sin f_i t = \cos(f_c - f_i)\, t - \cos(f_c + f_i)\, t. \quad (1)$$

The above equation indicates that the product of two sinusoids of frequencies f_c, f_i results in cosine waves of frequencies $f_c + f_i, f_c - f_i$. We note that two frequency shifts f_i and $-f_i$ are generated with respect to the carrier frequency f_c. Context recognition is achieved by observing the existence of either f_i or $-f_i$.

4.2 Frequency Shift Detection

To detect the frequency shift of the backscattered signal, we obtain time-series of the signal power spectrum by STFT (Short-time Fourier Transform). We then apply a moving average filter both in the time and frequency domains for smoothing. The window sizes of the moving average filter in the time and frequency domains are empirically set to 10 and 2, respectively. **Figure 3** shows an example of the spectrum after smoothing. We set the carrier frequency to 2,480 MHz and generated a frequency shift of 500 kHz. We see that a peak due to the frequency shift occurs at ±500 kHz while the peak at +500 kHz is buried in the carrier signal envelope. Even in such a case, the proposed method is robust to noise because it is sufficient if one of the peaks at $f_c + f_i$ and $f_c - f_i$ is detected.

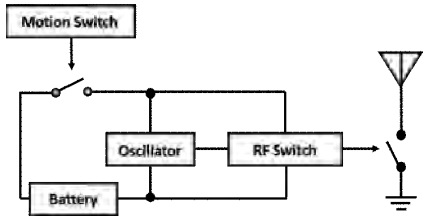

Fig. 2 Block diagram of frequency shift backscatter tag.

The details of the peak detection are as below. We let the signal level at frequency f be $P(f)$. In the following, we explain the detection of a peak of $f_c - f_i$. We note that the same applies to the case of $f_c + f_i$. We define the noise floor P_{floor} of the spectrum as below.

$$P_{floor} = P(f_c - f_i + \alpha/2). \quad (2)$$

Here, α is the width of the peak generated by the frequency shift. We empirically set α to 6 kHz.

Figure 3 shows the height of the signal level $\Delta P(f_c - f_i)$ of the shift frequency $f_c - f_i$ from P_{floor}. $\Delta P(f_c - f_i)$ is given as:

$$\Delta P(f_c - f_i) = P(f_c - f_i) - P_{floor}. \quad (3)$$

If $\Delta P(f_c - f_i)$ exceeds the threshold TH_P, the peak at $f_c - f_i$ is detected. If the peak of $f_c - f_i$ is detected, we recognize the occurrence of the context c_i associated with the backscatter tag i. However, some slight offset may occur due to the hardware imperfection (e.g., oscillation frequency offset). Therefore, we allow a slight shift around the target shift frequency. For this purpose, we introduce a window size f_δ in the frequency. $\Delta P(f_c - f_i)$ is then defined as the highest peak in the range of $[f_c - f_i - f_\delta, f_c - f_i + f_\delta]$. $\Delta P(f_c - f_i)$ changes according to the relative positions between the exciter, the backscatter tag, and the receiver. Therefore, we investigate the factors on the value of TH_P in Section 5.2.

4.3 Generating Carrier Signal by BLE

In Wi-Fi and Bluetooth used in many devices, a bandwidth of several MHz to several tens of MHz is assigned to each channel. For example, IEEE 802.11ax defines a channel width of 20 MHz to 80 MHz according to the transfer rate. The channel width of BLE is 2 MHz. To extend the range of the backscatter signal by the backscatter tag, it is desirable to avoid interference with the carrier signal transmitted from the exciter. This means it is desirable to send the carrier signal as narrow as possible. Therefore, we use the method proposed in Interscatter [7] for narrow-band carrier signal generation by BLE.

Figure 4 shows BLE channel assignment. BLE has 40 channels in the 2.4 GHz band with 2 MHz of the channel width. BLE

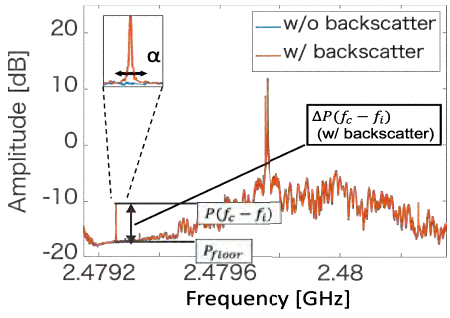

Fig. 3 Peak detection.

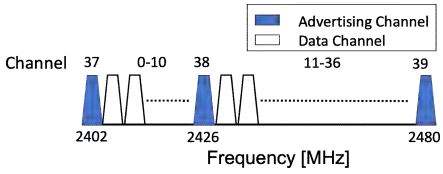

Fig. 4 BLE channel assignment.

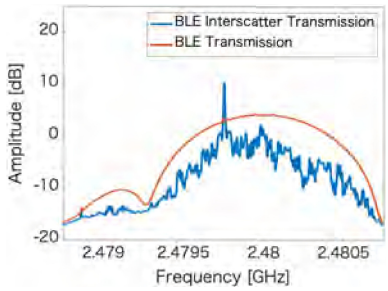

Fig. 5 Narrowband carrier generation by BLE.

uses GFSK (Gaussian Frequency-Shift Keying) for modulation. In GFSK, the frequency shifts by ±250 kHz from the center frequency of the channel correspond to the bits '1' and '0'. The three BLE channels, 37, 38, and 39, are called advertising channels and are used to establish a connection between devices. After the connection is established, the remaining 37 data channels are used for frequency hopping communication.

From the above BLE mechanism, Interscatter [7] generates a narrow-band carrier signal by always sending '0' s or '1' s in a single advertising channel. We employ the above technique to generate the narrow-band carrier signal by BLE. For implementation, we used a BLE evaluation board LAUNCHXL-CC1352P-2 from Texas Instruments. **Figure 5** shows the spectrum of the carrier signal generated on channel 39 whose center frequency is 2,480 MHz. The output power of the signal was set at 20 dBm, which is the maximum of the board, and the carrier signal was generated at a frequency shifted by 250 kHz in the negative direction by continuously sending '0' s. We see a carrier signal with a narrower bandwidth and a higher peak compared with a normal BLE signal. We also see the stronger signal in the frequency band above the peak. This is due to a carrier signal shifted in the negative direction from the center frequency of the BLE channel. As mentioned earlier, frequency shifts appear at positive and negative sides centered at the carrier frequency. To avoid an interference due to the carrier envelope, we observe the frequency shift farther from the center frequency of the BLE channel.

We note that BLE allows a frequency offset up to ±75 kHz and a frequency drift up to ±40 kHz in a single packet. Therefore, a frequency shift on the order of kHz is insufficient for identification. For this problem, one of the solutions is to detect the BLE carrier frequency first and to see the frequency difference from the detected BLE carrier frequency. However, in this paper, we focus on the sensing aspect of our method and leave the detailed design of identification of multiple tags for our future work. In the following evaluation, we assume that we can correctly identify the backscatter tags.

5. Evaluation

5.1 Evaluation Environment

To evaluate the performance of the backscatter tag, we have conducted experiments in a real environment. The software-defined radio USRP B210 was used as a receiver. Since the carrier signal generated by BLE has an envelope with a width of around 700 kHz, the oscillation frequency should be 350 kHz or more. Therefore, we set the sampling rate of USRP to 1.2 MHz. Since

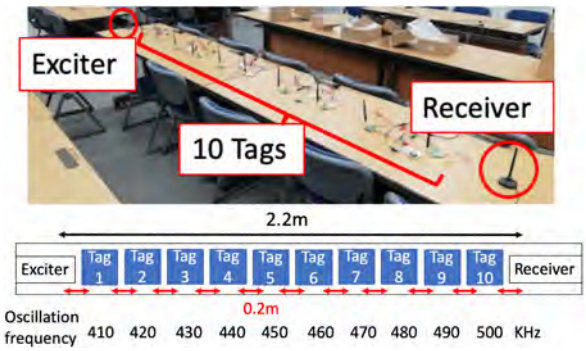

Fig. 6 Layout of multiple tags experiment.

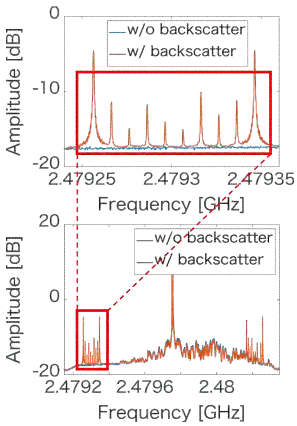

Fig. 7 Spectrum in multiple tags experiment.

BLE has a packet transmission interval, the FFT window size was set to 8,192, which is sufficiently larger than the BLE transmission interval. We used omnidirectional antennas with a gain of 2 dBi for the tag, the USRP, and the exciter. We generated the carrier signal by BLE channel 39 (center frequency 2,480 MHz) unless otherwise specified. In the experiment, instead of the oscillators, we used a signal generator Kuman FY6600 to easily change the oscillation frequency. We used EVAL-ADG902EBZ of Analog Devices as the RF switch and a CR2032 coin cell as a power supply.

5.2 Detection of Multiple Tags

To confirm the performance of the frequency shift detection, we deployed ten tags between the exciter and the receiver, as shown in **Fig. 6**. We set the oscillation frequency of the tag closest to the exciter to 410 kHz. We then increased the frequency of the next tag in steps of 10 kHz. We continued to transmit the carrier signal and kept the motion switches on. We have calculated the average power spectrum for 10 seconds.

The spectrum in **Fig. 7** shows multiple peaks around the shift frequencies. This means we can identify different tags by associated frequencies. However, as we mentioned in Section 4.3, we do not consider the influence of the BLE carrier frequency offset and drift in this paper. **Figure 8** shows the recall and precision of the peak detection for tags placed at each distance. We note that the distance between the exciter and the receiver is 2.2 m. The quality of the signal observed at the receiver depends on the exciter-tag distance, the tag-receiver distance, and the exciter-receiver distance. Therefore, recall and precision do not always

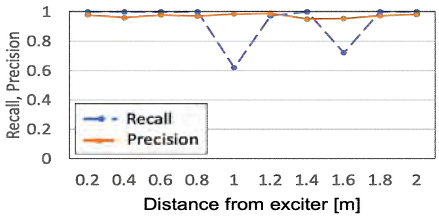

(a) $TH_P = 2$

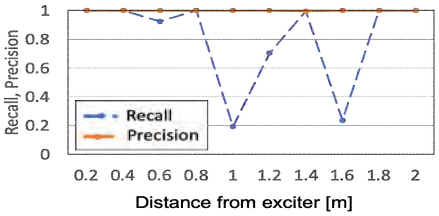

(b) $TH_P = 3$

Fig. 8 Recall and precision (Inter-tag distance = 20 cm).

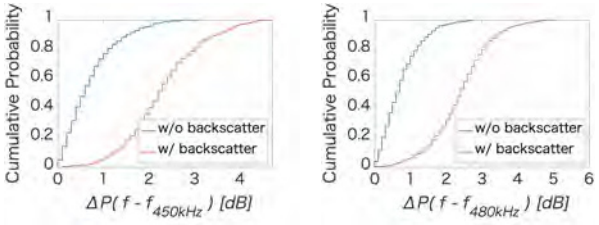

(a) 1 m (450 kHz) (b) 1.6 m (480 kHz)

Fig. 9 CDF of the signal level at shift frequency.

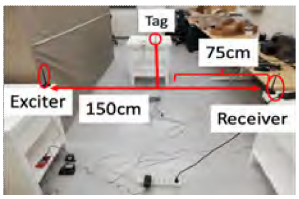

Fig. 10 Layout of single tag experiment.

decrease as the distance from the exciter increases. Since precision is almost 1 in most cases, we rarely find false positives. We also see a decrease of recall at 1 m and 1.6 m. When the observation of the frequency shift is difficult, false negatives increase, leading to a decrease of recall. The cause of the decrease of recall is fading since it is not linear to the distance and specific to 1 m and 1.6 m. The peak detection threshold $TH_P = 2$ achieves higher recall than $TH_P = 3$.

For detailed analysis, **Fig. 9** shows the cumulative frequency distribution (CDF) of peak levels at the shift frequencies by the tags with low recall and/or precision. The farther the CDFs of the two curves are, the higher the peak detection performance is. From the result in Fig. 9, we see that a larger TH_P increases the false negative rate, while a smaller TH_P increases the false positive rate, which is a trade-off. From the above results, $TH_P = 2$ is used in the following evaluation.

5.3 Sensing Range

To confirm the effect of the placement of the exciter, the receiver, and the tag, we conducted an experiment as shown in **Fig. 10**. The distance between the exciter and the receiver was

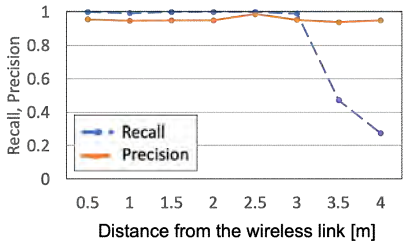

Fig. 11 Result of single tag experiment.

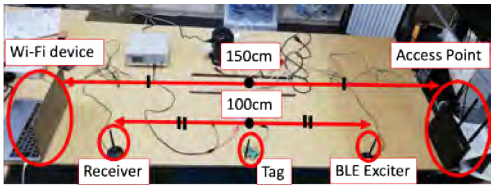

Fig. 12 Layout of Wi-Fi interference experiment.

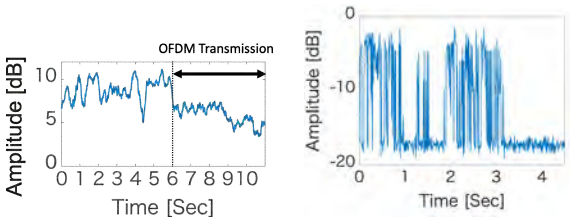

(a) Backscatter peak level during UDP communication (b) Wi-Fi signal level during video streaming

Fig. 13 Effect of Wi-Fi communication.

fixed at 1.5 m. We then placed the tag at different positions on the perpendicular bisector of the segment connecting the exciter and the receiver. **Figure 11** shows that the recall was more than 0.9 when the distance is shorter than 3 m. On the other hand, when the tag is placed farther than 3.5 m, the recall is less than 0.5. This is because the carrier signal from the exciter and the backscattered signal from the tag attenuated with the distance increase. When the distance is 3 m, the distance between the tag and the exciter/receiver is approximately 3 m. The above results indicate that we can recognize the context of the tag when both of the exciter-tag and tag-receiver distance are within 3 m.

5.4 Wi-Fi Interference

To investigate the performance under interference by Wi-Fi communication, we placed a Wi-Fi device and an access point, as shown in **Fig. 12**. We set the Wi-Fi communication channel to 4 (center frequency 2,427 MHz), which overlaps with the peak frequency generated by the backscatter tag. Intermittent Wi-Fi traffic was generated by continuously transmitting UDP packets from the Wi-Fi device. The exciter's carrier signal was set to the BLE channel 38 with the center frequency of 2,426 MHz. **Figure 13** (a) shows the time series of the signal level at the shift frequency. We started OFDM transmission at 6 seconds. We clearly see that the peak level at the shift frequency decreases during Wi-Fi transmission. The result indicates the difficulty of peak detection under Wi-Fi interference.

However, typical applications do not always transmit the packets. Figure 13 (b) shows the signal level at 2,411.7 MHz in the Wi-Fi channel when watching a YouTube live. The traffic shows

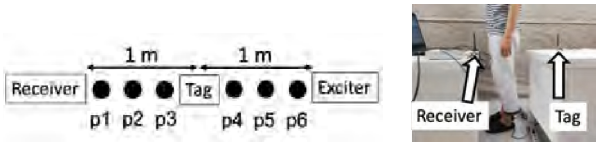

(a) Layout (b) Snapshot of shadowing experiment

Fig. 14 Shadowing effect experiment.

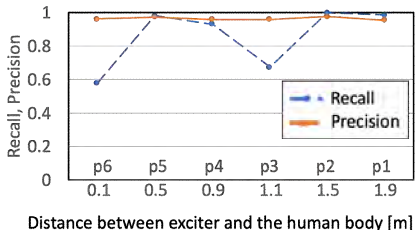

Fig. 15 Shadowing effect on recall and precision.

Table 1 Energy consumption of backscatter tag.

Component	Energy consumption [μA]
RF switch	1.0
Oscillator	10.0
Total	11.0

bursts of transmissions with intervals. We can still observe the frequency shift by the backscatter tag during the intervals of the bursty traffic. For example, even in the presence of Wi-Fi traffic, the frequency shift can be observed once every few seconds, which is still applicable to some applications. It is also possible to apply the RTS/CTS mechanism to reserve time slots for the monitoring of the frequency shift.

5.5 Effect of Shadowing

We evaluated the shadowing effect due to the human body. As shown in **Fig. 14** (a), the distance between the exciter and the receiver was fixed at 2 m, and the tag was placed at the midpoint. Then, a person stood at 6 positions shown by black dots in Fig. 14 (a) on the line-of-sight. Figure 14 (b) shows the snapshot of the experiment.

The result is shown in **Fig. 15**. When the person stood at p3 (10 cm from the tag) and p6 (10 cm from the exciter), the recall is less than 0.7. On the other hand, the recall exceeds 0.9 at the other positions. Compared with the other positions, at p3 and p6, the carrier signal and the backscattered signal are blocked by the human body immediately after transmission from the exciter and the tag. On the other hand, at the other positions, even if the line-of-sight is blocked, the carrier signal and the backscattered signal reach the tag and the receiver due to the diffraction and the reflection by surrounding objects such as walls and desks. For this reason, the shadowing effect is large if the signal is blocked immediately after the transmission or the backscatter.

5.6 Energy Consumption

Table 1 shows the estimated energy consumption of the backscatter tag calculated from the data sheets of each component. For the oscillator, we refer to a low-power oscillator SiT1569. Since the energy consumption is μW-order, the backscatter tag is expected to continue working for more than 2 years *without any sleep mode* approximately with a CR2032 coin cell (225 mAh). Furthermore, the backscatter tag is supposed to work forever with energy harvesting.

Table 2 Energy consumption of backscatter communication (MSP430F2013).

Transmission rate	Energy consumption [μA]
1 kbps	23.17
2 kbps	34.28
3 kbps	39.83

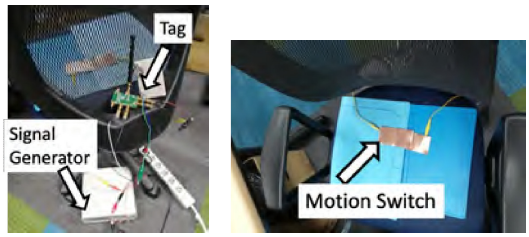

(a) Overview (b) Motion switch

Fig. 16 Seating sensor.

For comparison, we measured the energy consumption of backscatter communication using a low-power microcontroller MSP430F2013. In the comparison, we ignore the energy consumption of MEMS sensors since they are typically on the order of micro watts [*3]. In our implementation, the microcontroller switches the state of its pin according to a configured transmission rate, assuming the state of the pin indicates either a reflective or absorptive state of the antenna. We assumed FM0 coding according to the original implementation of ambient backscatter [6]. We note that the microcontroller goes back to the sleep mode after waking up to switch the pin state for saving energy consumption as much as possible.

Table 2 lists the energy consumption of backscatter communication for different transmission rates. It is clear that higher transmission rates require more energy because of the frequent wake-ups of the microcontroller. According to Ref. [36], typical activity recognition using a 3-axis accelerometer needs a sampling rate higher than 25 Hz. If we assume a float data type (4 bytes) for acceleration samples, the data generation rate is approximately 2.4 kbps. This means backscatter communication requires 34–39 μA to transmit the measured data. Therefore, the energy consumption of the backscatter tag is less than half of backscatter communication. We also note that the energy consumption of the backscatter tag can be further reduced according to the state of the motion switch.

5.7 Concept Applications

5.7.1 Seating Sensor

As one of the concept applications, we have implemented a seating sensor as shown in **Fig. 16** (a). When seated, the motion switch (see Fig. 16 (b)) is turned on, and the frequency shift appears in the backscattered signal.

We deployed an exciter and a receiver as shown in **Fig. 17**. The tag is placed on the back of the chair, and the exciter is placed in a

[*3] For example, an ultra low power accelerometer Analog Devices ADXL362 consumes 3.6 μW in the active mode according to the data sheet.

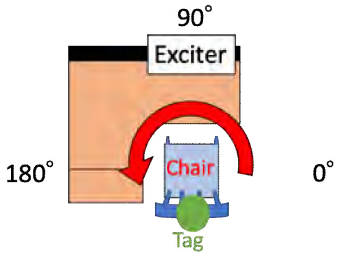

Fig. 17 Layout of seating sensor experiment.

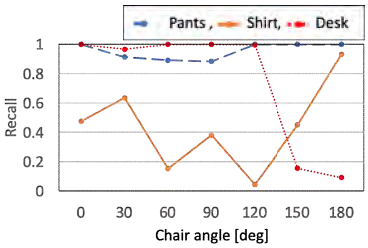

(a) Recall

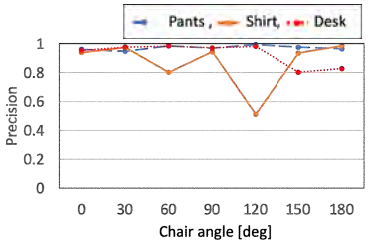

(b) Precision

Fig. 18 Recall and precision of seating sensor.

position that assumes a router. The distance between the tag and the exciter is 1.4 m. Assuming that the receiver is a smartphone, data was acquired in three positions: left chest pocket, right pants pocket, and desk (180° direction). To evaluate the influence of the human body sitting on the chair, the person sat at different chair angles as shown in Fig. 17 and acquired data in 30° increments from 0° to 180°.

Figure 18 shows the evaluation results. When the receiver was in the pants pocket, the recall was about 0.8 at all angles. This is mainly because the position of the pants pocket was close to the tag. On the other hand, when the receiver was in the chest pocket, the recall was less than 0.8 except for the angle of 180°. This is because the backscattered signal was blocked by the human body between the tag and the receiver. For the angle of 180°, the recall exceeded 0.8 because the shadowing effect was small due to the position relation between the receiver, the tag, and the body. When the receiver was placed on the desk, the recall was more than 0.9 at angles less than 120°. In contrast, the recall decreased at 150° and 180°. This is because the body between the receiver and the tag blocked the backscattered signal as in the case of the chest pocket. From the above results, we found that the placement of the tag and the receiver should be carefully designed to avoid the shadowing due to the human body.

5.7.2 Pedometer

We implemented a pedometer as shown in **Fig. 19** (a). A low-power oscillator SiT1569 was used with the oscillation frequency of 393 kHz. Figure 19 (b) shows the motion switch. The motion switch is turned on when the foot lands on the floor while it is turned off when the foot leaves the floor. Therefore, the existence/absence of the frequency shift indicates the states of the foot landing/leaving. In some cases, false negatives of the frequency shift can occur owing to moving out of sensing range and shadowing. The effect of such false negatives can be mitigated by applying a simple filter based on motion periodicity. We leave further investigation on such application-specific designs out of scope of this paper.

(a) Overview (b) Motion switch

Fig. 19 Pedometer.

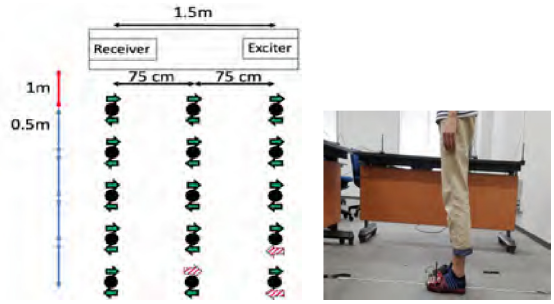

(a) Layout and result: arrows indicate the direction of the person. The colors indicate success (green) or failure (red) in detection.

(b) Snapshot of pedometer experiment

Fig. 20 Pedometer experiment.

Figure 20 (a) shows the experiment layout to see the performance of the pedometer. We placed the exciter and the receiver on two desks 1.5 meters apart. A person put the pedometer slipper on the left foot and stood on the 15 positions shown in Fig. 20 (a). The person faced to the left side or the other side in Fig. 20 (a). Figure 20 (b) shows the snapshot of the experiment.

Figure 20 (a) also shows the results of the peak detection at each position for each direction. In the figure, arrows indicate the direction of the person. The colors of the arrows also indicate success or failure in the peak detection. We see that the peak detection fails at 3 positions far from the receiver. This result is consistent with the result in Section 5.3, considering the height from the foot to the antenna on the desk. We also found that the shadowing effect due to the leg is limited because it is smaller than the body.

6. Conclusion

In this paper, we proposed BAAS, a novel platform for wireless context sensing. We designed and evaluated the frequency shift backscatter tag to achieve context recognition with ultra-low power consumption. Unlike conventional backscatter for communication purposes, BAAS uses backscatter as a sensor to recognize context. As a result of the performance evaluation, we found that we can recognize the context by the tag if the exciter-tag and

the tag-receiver distance are within 3 m. For future work, we are planning to design a method to identify multiple tags considering the BLE frequency offset and drift. We also plan to develop a backscatter tag combined with energy harvesting to demonstrate ever-lasting sensors for context recognition. Another future work is to analyze the backscattered signal according to its movement for detailed motion sensing.

Acknowledgments This work was partly supported by JST, PRESTO Grant Number JPMJPR1932, and JSPS KAKENHI 19K11941, JP20K20398, and JP19H05665, Japan.

References

[1] Chesser, M., Jayatilaka, A., Visvanathan, R., Fumeaux, C., Sample, A. and Ranasinghe, D.C.: Super Low Resolution RF Powered Accelerometers for Alerting on Hospitalized Patient Bed Exits, *Proc. IEEE International Conference on Pervasive Computing and Communications* (*PerCom*), pp.1–10 (2019).

[2] Ohara, K., Maekawa, T. and Matsushita, Y.: Detecting State Changes of Indoor Everyday Objects Using Wi-Fi Channel State Information, *Proc. ACM on Interactive, Mobile, Wearable and Ubiquitous Technologies*, Vol.1, No.3, pp.1–28 (2017).

[3] Mshali, H., Lemlouma, T., Moloney, M. and Magoni, D.: A Survey on Health Monitoring Systems for Health Smart Homes, *International Journal of Industrial Ergonomics*, Vol.66, pp.26–56 (2018).

[4] Lara, O.D. and Labrador, M.A.: A Survey on Human Activity Recognition using Wearable Sensors, *IEEE Communications Surveys Tutorials*, Vol.15, No.3, pp.1192–1209 (2013).

[5] Hoseini-Tabatabaei, S.A., Gluhak, A. and Tafazolli, R.: A Survey on Smartphone-Based Systems for Opportunistic User Context Recognition, *ACM Comput. Surv.*, Vol.45, No.3, pp.1–51 (2013).

[6] Liu, V., Parks, A., Talla, V., Gollakota, S., Wetherall, D. and Smith, J.R.: Ambient Backscatter: Wireless Communication out of Thin Air, *SIGCOMM Computer Communication Review*, Vol.43, No.4, pp.39–50 (2013).

[7] Iyer, V., Talla, V., Kellogg, B., Gollakota, S. and Smith, J.: Inter-Technology Backscatter: Towards Internet Connectivity for Implanted Devices, *Proc. 2016 ACM SIGCOMM Conference*, pp.356–369, ACM (online), DOI: 10.1145/2934872.2934894 (2016).

[8] Kellogg, B., Parks, A., Gollakota, S., Smith, J.R. and Wetherall, D.: Wi-Fi Backscatter: Internet Connectivity for RF-Powered Devices, *SIGCOMM Computer Communication Review*, Vol.44, No.4, pp.607–618 (online), DOI: 10.1145/2740070.2626319 (2014).

[9] Bao, L. and Intille, S.S.: Activity recognition from user-annotated acceleration data, *Proc. 2nd International Conference on Pervasive Computing* (*Pervasive 2004*), pp.1–17 (2004).

[10] Sankaran, K., Zhu, M., Guo, X.F., Ananda, A.L., Chan, M.C. and Peh, L.-S.: Using mobile phone barometer for low-power transportation context detection, *Proc. 12th ACM Conference on Embedded Network Sensor Systems* (*SenSys '14*), pp.191–205 (2014).

[11] Nakajima, Y., Murao, K., Terada, T. and Tsukamoto, M.: A method for energy saving on context-aware system by sampling control and data complement, *Proc. International Symposium on Wearable Computers* (*ISWC*), pp.1–4 (2010).

[12] Khalifa, S., Hassan, M. and Seneviratne, A.: Pervasive self-powered human activity recognition without the accelerometer, *IEEE International Conference on Pervasive Computing and Communications* (*PerCom*), pp.79–86 (2015).

[13] Ma, Y., Zhou, G. and Wang, S.: WiFi Sensing with Channel State Information: A Survey, *ACM Comput. Surv.*, Vol.52, No.3 (online), DOI: 10.1145/3310194 (2019).

[14] Liu, J., Liu, H., Chen, Y., Wang, Y. and Wang, C.: Wireless Sensing for Human Activity: A Survey, *IEEE Communications Surveys Tutorials*, Vol.22, No.3, pp.1629–1645 (2020).

[15] Wang, Y., Liu, J., Chen, Y., Gruteser, M., Yang, J. and Liu, H.: E-eyes: Device-free Location-oriented Activity Identification Using Fine-grained WiFi Signatures, *Proc. 20th Annual International Conference on Mobile Computing and Networking*, pp.617–628 (2014).

[16] Wang, W., Liu, A.X., Shahzad, M., Ling, K. and Lu, S.: Understanding and Modeling of WiFi Signal Based Human Activity Recognition, *Proc. 21st Annual International Conference on Mobile Computing and Networking*, pp.65–76 (2015).

[17] Palipana, S., Rojas, D., Agrawal, P. and Pesch, D.: FallDeFi: Ubiquitous Fall Detection Using Commodity Wi-Fi Devices, *Proc. ACM Interact. Mob. Wearable Ubiquitous Technol.*, Vol.1, No.4 (online), DOI: 10.1145/3161183 (2018).

[18] Zeng, Y., Wu, D., Xiong, J., Liu, J., Liu, Z. and Zhang, D.: MultiSense: Enabling Multi-Person Respiration Sensing with Commodity WiFi, *Proc. ACM Interact. Mob. Wearable Ubiquitous Technol.*, Vol.4, No.3 (online), DOI: 10.1145/3411816 (2020).

[19] Zheng, Y., Zhang, Y., Qian, K., Zhang, G., Liu, Y., Wu, C. and Yang, Z.: Zero-Effort Cross-Domain Gesture Recognition with Wi-Fi, *Proc. 17th Annual International Conference on Mobile Systems, Applications, and Services, MobiSys '19*, pp.313–325, Association for Computing Machinery (online), DOI: 10.1145/3307334.3326081 (2019).

[20] Guo, X., Liu, J., Shi, C., Liu, H., Chen, Y. and Chuah, M.C.: Device-Free Personalized Fitness Assistant Using WiFi, *Proc. ACM Interact. Mob. Wearable Ubiquitous Technol.*, Vol.2, No.4 (online), DOI: 10.1145/3287043 (2018).

[21] Ding, J. and Chandra, R.: Towards Low Cost Soil Sensing Using Wi-Fi, *The 25th Annual International Conference on Mobile Computing and Networking, MobiCom '19*, Association for Computing Machinery (online), DOI: 10.1145/3300061.3345440 (2019).

[22] Yu, Y., Wang, D., Zhao, R. and Zhang, Q.: RFID Based Real-Time Recognition of Ongoing Gesture with Adversarial Learning, *Proc. 17th Conference on Embedded Networked Sensor Systems, SenSys '19*, pp.298–310, Association for Computing Machinery (online), DOI: 10.1145/3356250.3360045 (2019).

[23] Wang, C., Liu, J., Chen, Y., Xie, L., Liu, H.B. and Lu, S.: RF-Kinect: A Wearable RFID-Based Approach Towards 3D Body Movement Tracking, *Proc. ACM Interact. Mob. Wearable Ubiquitous Technol.*, Vol.2, No.1 (online), DOI: 10.1145/3191773 (2018).

[24] Jin, H., Yang, Z., Kumar, S. and Hong, J.I.: Towards Wearable Everyday Body-Frame Tracking Using Passive RFIDs, *Proc. ACM Interact. Mob. Wearable Ubiquitous Technol.*, Vol.1, No.4 (online), DOI: 10.1145/3161199 (2018).

[25] Wang, C., Xie, L., Wang, W., Chen, Y., Bu, Y. and Lu, S.: RF-ECG: Heart Rate Variability Assessment Based on COTS RFID Tag Array, *Proc. ACM Interact. Mob. Wearable Ubiquitous Technol.*, Vol.2, No.2 (online), DOI: 10.1145/3214288 (2018).

[26] Xie, B., Xiong, J., Chen, X., Chai, E., Li, L., Tang, Z. and Fang, D.: Tagtag: Material Sensing with Commodity RFID, *Proc. 17th Conference on Embedded Networked Sensor Systems, SenSys '19*, pp.338–350, Association for Computing Machinery (online), DOI: 10.1145/3356250.3360027 (2019).

[27] Wang, J., Chang, L., Aggarwal, S., Abari, O. and Keshav, S.: Soil Moisture Sensing with Commodity RFID Systems, *Proc. 18th International Conference on Mobile Systems, Applications, and Services, MobiSys '20*, pp.273–285, Association for Computing Machinery (online), DOI: 10.1145/3386901.3388940 (2020).

[28] Varshney, A., Harms, O., Penichet, C.-P., Rohner, C., Hermans, F. and Voigt, T.: LoRea: A backscatter architecture that achieves a long communication range, *Proc. 15th ACM Conference on Embedded Network Sensor Systems* (*SenSys '17*) (2017).

[29] Parks, A.N., Liu, A., Gollakota, S. and Smith, J.R.: Turbocharging ambient backscatter communication, *Proc. ACM Conference on SIGCOMM*, pp.619–630 (2014).

[30] Kellogg, B., Talla, V., Gollakota, S. and Smith, J.R.: Passive Wi-Fi: Bringing Low Power to Wi-Fi Transmissions, *Proc. 13th Usenix Conference on Networked Systems Design and Implementation* (*NSDI '16*), pp.151–164 (2016).

[31] Iyer, V., Chan, J. and Gollakota, S.: 3D Printing Wireless Connected Objects, *ACM Trans. Graphics* (*TOG*) (2017).

[32] Gao, C., Li, Y. and Zhang, X.: LiveTag: Sensing Human-Object Interaction Through Passive Chipless Wi-Fi Tags, *GetMobile: Mobile Comp. and Comm.*, Vol.22, No.3, pp.32–35 (online), DOI: 10.1145/3308755.3308766 (2019).

[33] Waghmare, A., Xue, Q., Zhang, D., Zhao, Y., Mittal, S., Arora, N., Byrne, C., Starner, T. and Abowd, G.D.: UbiquiTouch: Self Sustaining Ubiquitous Touch Interfaces, *Proc. ACM Interact. Mob. Wearable Ubiquitous Technol.*, Vol.4, No.1 (online), DOI: 10.1145/3380989 (2020).

[34] Daskalakis, S.-N., Assimonis, S., Kampianakis, E. and Bletsas, A.: Soil Moisture Scatter Radio Networking With Low Power, *IEEE Trans. Microwave Theory and Techniques*, Vol.64, No.7, pp.2338–2346 (2016).

[35] Ranganathan, V., Gupta, S., Lester, J., Smith, J.R. and Tan, D.: RF Bandaid: A Fully-Analog and Passive Wireless Interface for Wearable Sensors, *Proc. ACM Interact. Mob. Wearable Ubiquitous Technol.*, Vol.2, No.2 (online), DOI: 10.1145/3214282 (2018).

[36] Bulling, A., Blanke, U. and Schiele, B.: A Tutorial on Human Activity Recognition Using Body-Worn Inertial Sensors, *ACM Computing Surveys*, Vol.46, No.3 (online), DOI: 10.1145/2499621 (2014).

Editor's Recommendation

This paper shows a design and implementation of a context

recognition system that utilized backscatter as a sensor. The proposed method is simple, but highly useful, as it can be easily applied to different environments. In addition, it was evaluated with various types of situation recognition as the actual system, which is a promising result for future industrial applications. Thus it is selected as a recommended paper.

(Chief examiner of SIGDPS Atsushi Tagami)

Yoshihiro Nakagawa received his M.E. degree in Information and Computer Science from Osaka University, Japan in 2021. He works in the Kansai Electric Power Co., Inc since 2021.

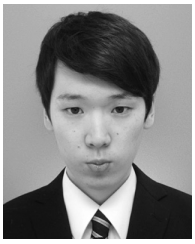

Toru Maeda received his M.E. degree in Information and Computer Science from Osaka University, Japan in 2020.

Akira Uchiyama received his M.E. and Ph.D. degrees in Information and Computer Science from Osaka University in 2005 and 2008, respectively. From 2009 to 2021, he had been an Assistant Professor at Graduate School of Information Science and Technology, Osaka University. He was a visiting scholar in the University of Illinois at Urbana-Champaign from 2008 to 2009 and a research fellow of the Japan Society for the Promotion of Science from 2007 to 2009. Since 2021, he is an Associate Professor at Osaka University. His current research interests include mobile sensing and applications in pervasive and ubiquitous computing. He is a member of IEEE, ACM, IEICE and IPSJ.

Teruo Higashino received his B.S., M.S. and Ph.D. degrees in Information and Computer Sciences from Osaka University, Japan in 1979, 1981 and 1984, respectively. He joined the faculty of Osaka University in 1984. From 2002 to 2021, he had been a Professor in Graduate School of Information Science and Technology at Osaka University. He has been a Specially Appointed Professor at Osaka University and a Professor at Kyoto Tachibana University since 2021. His current research interests include design and analysis of distributed systems, communication protocol and mobile computing. He is a senior member of IEEE, a fellow of Information Processing Society of Japan (IPSJ), and a member of ACM and IEICE of Japan.